Suppression of speckles at high adaptive correction using speckle symmetry

E. E. Bloemhof
Jet Propulsion Laboratory, California Institute of Technology,
Pasadena, CA USA 91109

ABSTRACT

Focal-plane speckles set important sensitivity limits on ground- or space-based imagers and coronagraphs that may be used to search for faint companions, perhaps ultimately including exoplanets, around stars. As speckles vary with atmospheric fluctuations or with drifting beamtrain aberrations, they contribute speckle noise proportional to their full amplitude. Schemes to suppress speckles are thus of great interest. At high adaptive correction, speckles organize into species, represented by algebraic terms in the expansion of the phase exponential, that have distinct spatial symmetry, even or odd, under spatial inversion. Filtering speckle patterns by symmetry may eliminate a disproportionate fraction of the speckle noise while blocking (only) half of the image signal from the off-axis companion being sought. The fraction of speckle power and hence of speckle noise in each term will vary with degree of correction, and so also will the net symmetry in the speckle pattern. Systematic numerical investigations are presented of the net symmetry of noise variance as a function of adaptive correction, i.e., Strehl ratio S, and deformable mirror actuator density D/a, where a is the deformable mirror actuator spacing referred to the pupil of diameter D, which controls the characteristic transverse spatial frequency of the wavefront. The degree of speckle symmetry is found to be substantial even at current relatively modest ground-based corrections (S=0.6, D/a=16 in the near-infrared). With parameters representative of "extreme" adaptive optics of the near future (S=0.99, D/a=100), the antisymmetric noise variance fraction is 0.99967 averaged over two Airy rings in the inner halo, so simple image processing (symmetry filtering) can improve the net speckle-noise-limited companion-detection SNR by a factor of about 28. Analogous processing can enhance SNR in coronagraphic searches, where speckle patterns before processing are predominantly symmetric.

Keywords: adaptive optics, speckles, atmospheric turbulence

1. INTRODUCTION: SPATIAL SYMMETRY IN HIGHLY CORRECTED IMAGES

Highly corrected adaptive images have halos of speckles (Fig. 1) whose fluctuations limit sensitive searches for faint companions around other stars[1-5]. Speckles are particularly troublesome, generating image noise proportional to their full intensity rather than the square root familiar with photon noise. Noise variance is[6]

$$\sigma^2 \approx \frac{F_s^{\,2}}{16}\frac{t}{\tau_0} \quad , \tag{1}$$

where the typical single-speckle intensity is F_s, the coherence time is τ_0, and the integration time is t. At high correction, the short-exposure image intensity from a particular phase screen realization is approximately[4]

$$I(x,y) = \left|\overline{A\exp(i\phi)}\right|^2 \approx \left|\overline{A} + i\,\overline{\phi}\right|^2 \approx \left|\overline{A}\right|^2 + 2\,\mathrm{Re}\left\{ i\,\overline{A}^{*}\,\overline{\phi} \right\} + \left|\overline{\phi}\right|^2 \quad . \tag{2}$$

The overbar denotes two-dimensional (spatial) Fourier transformation, the asterisk denotes complex conjugation, A is the aperture function (here A=1 or 0 in this simple illustration treating phase speckles only), and ϕ is the remnant pupil-plane phase aberration. The first term on the right side, $|\overline{A}|^2$, is the point-spread function (PSF), an Airy pattern for a circular aperture:

$$PSF(x,y) = \left| \bar{A} \right|^2 = Airy = \left[\frac{2J_1(\pi D\theta/\lambda)}{\pi D\theta/\lambda} \right]^2 \quad . \tag{3}$$

Here D is the pupil diameter, λ is the wavelength of observation, and θ is the radial coordinate of the Airy pattern.

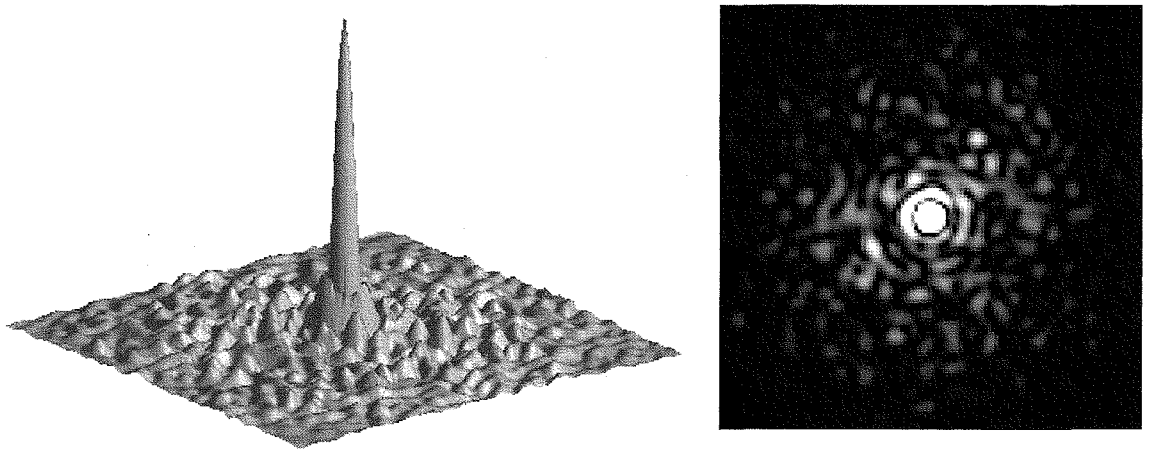

Figure 1 – Spatial symmetries of speckles in a highly corrected monochromatic short-exposure image, numerically simulated, representative of the current ground-based state of the art in adaptive imaging (S=0.60, D/a=16). The image spans a field measuring 30 λ/D x 30 λ/D. (Left) Three-dimensional perspective with an exaggerated vertical scale shows a diffraction-limited core surrounded by a speckle halo ~λ/a in diameter containing total fractional image power ~(1-S). (Right) The same image plotted as a two-dimensional grayscale displays some antisymmetric structure on the inner Airy rings, where the Airy amplitude factor $\bar{A}$ and so speckles from the linear term of Equation (2) are brightest (cf. the innermost ring has a bright and dark speckle pair to the left and right of center). In the outer halo, Airy rings are fainter and not clearly seen, implying $|\bar{A}| < |\bar{\phi}|$, which further implies that speckles from the quadratic term of Equation (2) dominate those from the linear term and the antisymmetry is washed out. Quantitative analysis shows (Fig. 4) the antisymmetric speckle noise variance fraction in the inner Airy rings at this correction is ~0.7.

The expansion in Equation (2) describes the dominant (brightest) phase speckles; amplitude speckles may easily be included by considering the generalization from A to A+δA in the algebraic expansion of Equation (2), where δA captures the effect of slight transmission defects in the optics. The two speckle terms in Equation (2) are respectively linear and quadratic in "speckle amplitude" $\bar{\phi}$; they are also spatially antisymmetric and symmetric, respectively, as may be derived in a straightforward way from the fact that real functions A, ϕ have hermitian Fourier transforms[7]. Though other, fainter speckle terms are included in the numerical simulations to be presented in §3, the interplay between the two terms in Equation (2) gives insight into the dependence of net speckle symmetry with correction and with position in the halo. Those dependencies arise because typical peak intensities depend on correction through its effect on $\bar{\phi}$ and, for the linear term, on position within the halo through the Airy amplitude $\bar{A}$. Airy amplitude is given by the square root of Equation (3); the typical peak of speckle amplitude may be estimated as roughly[4]

$$\left|\bar{\phi}\right|_{typ} \approx \sqrt{\frac{(1-S)}{0.342}\left(\frac{a}{D}\right)} \tag{4}$$

relative to the peak of $|\bar{A}|$. Equation (4) provides a basis for convenient analytic estimation of typical brightness of the two key speckle species. The key parameters controlling speckle intensity are Strehl ratio S, deformable mirror actuator density D/a, and, for the linear term, position within the speckle halo.

Equation (4) estimates typical peak speckle intensities to within a factor ~2 by equally dividing the speckle power, (1-S), among $N=0.342(D/a)^2$ speckles[8]. Speckles from the linear term $2\,\mathrm{Re}\{i\bar{A}^*\bar{\phi}\}$ are "pinned" to (localized on) PSF rings[9] through the factor $\bar{A}$; quadratic speckles $|\bar{\phi}|^2$ roam freely. The linear term is of lower order in $\bar{\phi}$, so dominates the image when correction is so high (S→1, D/a large) that $\bar{\phi}$ is smaller in amplitude than $\bar{A}$; the latter amplifies $\bar{\phi}$ to produce linear-term speckles. In this situation (cf. the outer parts of Fig. 2), quadratic speckles $|\bar{\phi}|^2$ are faint enough to sink beneath local Airy rings of $|\bar{A}|^2$, so Airy nulls are no longer washed out. The now-distinct rings show an antisymmetric pattern of brighter and dimmer knots due to linear-term speckles.

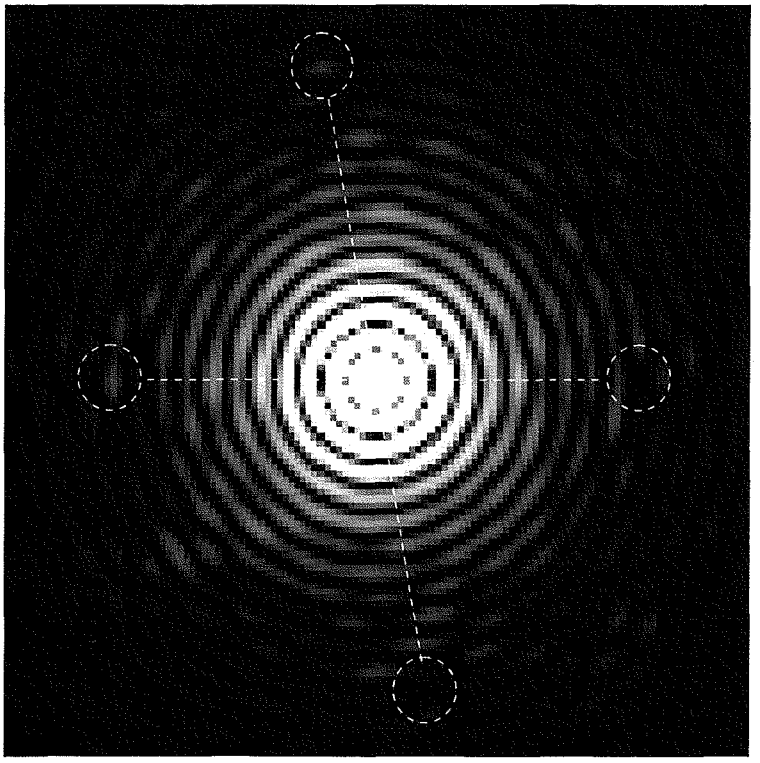

Figure 2 – Emergence of antisymmetric speckles with increasing correction. The image spans 30 λ/D x 30 λ/D, and is computed for a very high correction S=0.99, D/a=32. As is clear in this Figure and can be verified from Equations (3) and (4), the typical peak speckle amplitude $\bar{\phi}$ for such high correction is smaller than the Airy amplitude $\bar{A}$ even out to the 14 or 15 Airy rings shown here. So antisymmetric speckles "pinned", or localized, on Airy rings dominate; examples on the 10th and 12th rings are circled.

At high correction, because the linear term dominates, the spatially antisymmetric speckle noise variance fraction approaches unity. Simple image processing can be used to suppress speckle noise of either chosen symmetry. Symmetric/antisymmetric noise is removed[2,3,10] by subtracting/adding to an image a copy of itself rotated 180°. Half the signal is also lost, because any off-axis companion consists of equal-amplitude symmetric and antisymmetric components (Fig. 3), so net imaging signal-to-noise ratio (SNR) improves only if one symmetry type produces at least 0.75 of the noise variance. Symmetrization (but not antisymmetrization) introduces a 180° position-angle ambiguity, of little scientific consequence. This speckle noise reduction works for any wavelength, and for speckles caused by amplitude variations δA over the pupil rather than by phase variations ϕ (for small δA, $2\delta A$ is the fractional intensity variation; brightest "amplitude" speckle terms are the spatially-symmetric $2\mathrm{Re}\{\overline{A}^{*}\overline{\delta A}\}$ and $|\overline{\delta A}|^2$, whose behavior is similar to that detailed here for phase speckles).

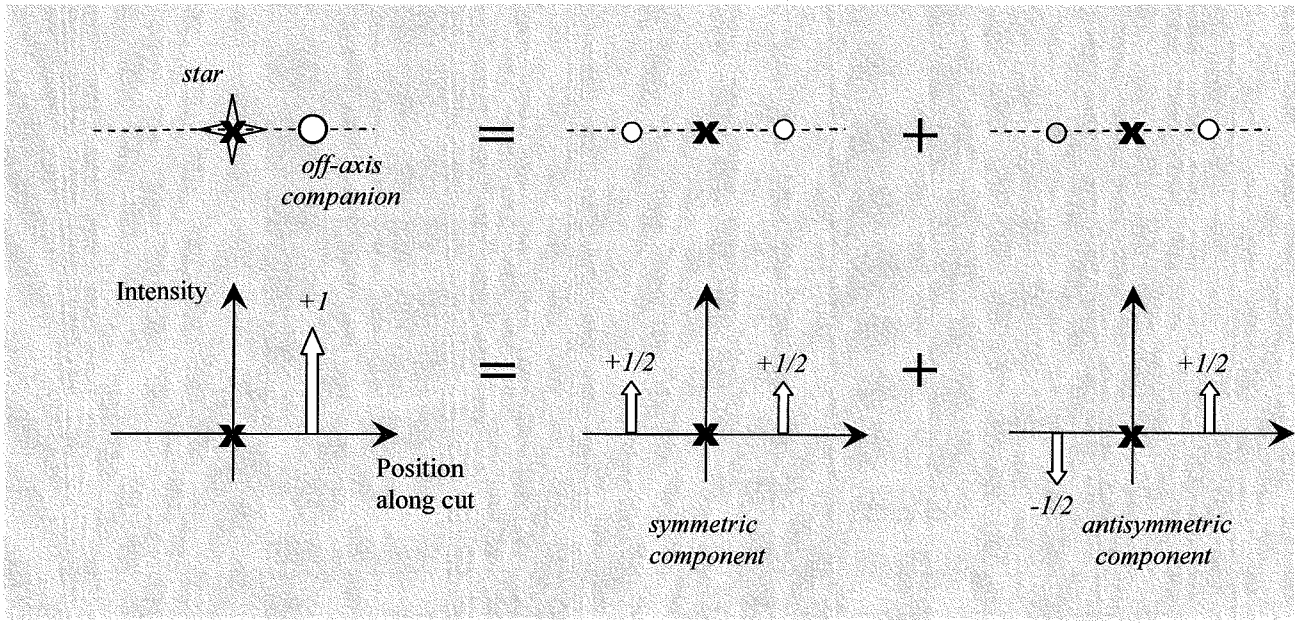

Figure 3 – Decomposition of an off-axis companion into symmetric and antisymmetric image components. The primary star is at the origin, and defines the imaging phase center ("**X**"). With respect to that position, an off-axis point source is mathematically equivalent to the sum of spatially symmetric and antisymmetric components of equal strength, as illustrated here. For simple imaging at high correction, the brightest speckles are antisymmetric, so filtering to select the symmetric image component will remove a disproportionately large fraction of the speckle noise. For coronagraphy, where antisymmetric speckles are suppressed, image antisymmetrization is generally desirable instead (§4).

The estimates given here for speckle intensity and noise, based on inserting Equation (4) for the speckle amplitude into the speckle terms of Equation (2), are larger than past estimates that have traditionally ignored the cross-term describing linear speckles. While that term contributes zero total image power[11], being spatially antisymmetric, it can have large local fluctuations that dominate speckle noise. (Negative linear-term intensities partially erode Airy rings to which they are pinned, keeping total intensity non-negative.) When $|\overline{A}|>|\overline{\phi}|$, as must occur at sufficiently high correction, the relatively large Airy amplitude substantially amplifies linear-term speckle intensity and noise above quadratic; this behavior can be seen by inspection in Fig. 2. In the following sections the amount of this excess of speckle noise will be quantified, and a simple means of removing it with image processing based on speckle symmetries will be presented.

2. NUMERICAL STUDY OF SPECKLE NOISE VARIANCE SYMMETRY FRACTION

The net symmetry content of the speckle halo is now explored numerically as a function of adaptive correction; this naturally controls the degree of speckle noise reduction achievable through symmetry-based image processing techniques. At each (S, D/a), 128 short-exposure images are generated by applying the full Fourier optical expression[12], $|\overline{A\exp(i\phi)}|^2$, to random residual pupil-plane phase screens, ϕ. (Equations (2) and (4) are not used in the calculations, but guide the interpretation.) The telescope pupil A is round, unobscured, and 128 pixels in diameter within a 1024x1024 grid space, so the image-plane pixels that result measure ~1/8(λ/D) on a side. From the 128 images, speckle noise is estimated at each pixel within the halo. To obtain representative values, the antisymmetric and symmetric components of speckle noise are separately averaged over all pixels lying within each of five spatial zones covering different radial regions of the halo, smoothing an expected radial dependence inherited from $\overline{A}$ in the linear term $2\,\mathrm{Re}\{i\overline{A}^{*}\,\overline{\phi}\}$. This dependence was already visible in Fig. 1 for correction roughly equal to the best yet achieved with ground-based adaptive optics. The five spatial zones are contiguous annuli lying between radial boundaries 1.22, 3.24, 5.24, 7.24, 9.25, and 11.25 λ/D; each encompasses two Airy rings. Results will be examined in detail for the innermost radial zone between 1.22 λ/D and 3.24 λ/D, i.e., between the 1st and 3rd Airy nulls.

Calculations will be presented in terms of monochromatic short exposures because these are the most primitive quantities from which realistic observations are built up. Speckle noise will generally be reduced in observations spanning broader spectral bandwidth; in these cases, speckle patterns form radial streaks, and the intensity on a single pixel in the image is akin to averaging over a radial range in a monochromatic speckle pattern. Speckle noise will also be smoothed in an obvious way by the area averaging performed by a detector spanning many of our numerical pixels. The effects of finite integration time may be computed with Equation (1). A ground-based instrument sees a fresh phase screen due to the turbulent atmosphere on a timescale substantially shorter than one second; but for a space-based observatory, the timescale for evolution of the phase screen may be rather long. Symmetry properties of the different speckle types are retained by coadditions of multiple short exposures.

Phase screens are computed in terms of independent local cells, rather than global modes. This seems physically most appropriate to space-based instruments, while capturing the essentials of ground-based systems as well. Each D/a-sized cell of the pupil/aperture plane is assigned a phase value that is randomly chosen according to a Gaussian probability distribution of zero mean and with one-sigma value related to the Strehl ratio by $\sqrt{(1-S)}$. (In practice, for many values of D/a a roughly equivalent computation is carried out in which primitive cells of the numerical grid are assigned random values, and the grid is then convolved to a spatial resolution ~D/a and rescaled to match the appropriate Strehl.) No connection is made in this procedure with the Kolmogorov statistics of the atmosphere. However, the key spatial scale of a ground-based adaptive optics system may be identified by setting $D/a = D/r_0$, where r_0 is the transverse coherence scale (Fried parameter).

3. RESULTS: SYMMETRY CONTENT VS. CORRECTION FOR SIMPLE IMAGING

Fixing D/a=16, representative of current high-order adaptive optics[13], Strehl values ranging from 0.1 to 0.999 are modelled. Speckle noise is averaged over image pixels lying within each of the five radial halo zones mentioned in the previous section. Fig. 4 gives the results for the innermost zone. The general behavior may be understood with the intensity estimates of Equations (2), (3), and (4). At high correction (S→1, D/a large), $\overline{\phi}$ becomes small, so terms with fewer powers of $\overline{\phi}$ dominate. This favors the antisymmetric linear term $2\,\mathrm{Re}\{i\overline{A}^{*}\,\overline{\phi}\}$ anywhere in the focal plane except precisely on Airy nulls ($\overline{A} = 0$), though it dominates first in the inner halo where $\overline{A}$ is relatively large. Thus at highest correction the noise variance approaches antisymmetry, particularly in the inner halo (Fig. 4). At intermediate Strehl, in the mid and outer halo, $|\overline{\phi}|$ exceeds $|\overline{A}|$ so that quadratic-term speckles $|\overline{\phi}|^2$ are brightest and speckle noise variance is moderately symmetric. Symmetry imbalances exceed the break-even threshold, 0.75, on inner Airy rings for S=0.7, D/a=16 (Fig. 4), so the seemingly random speckle halos of the best current adaptively-corrected images contain substantial spatial symmetry.

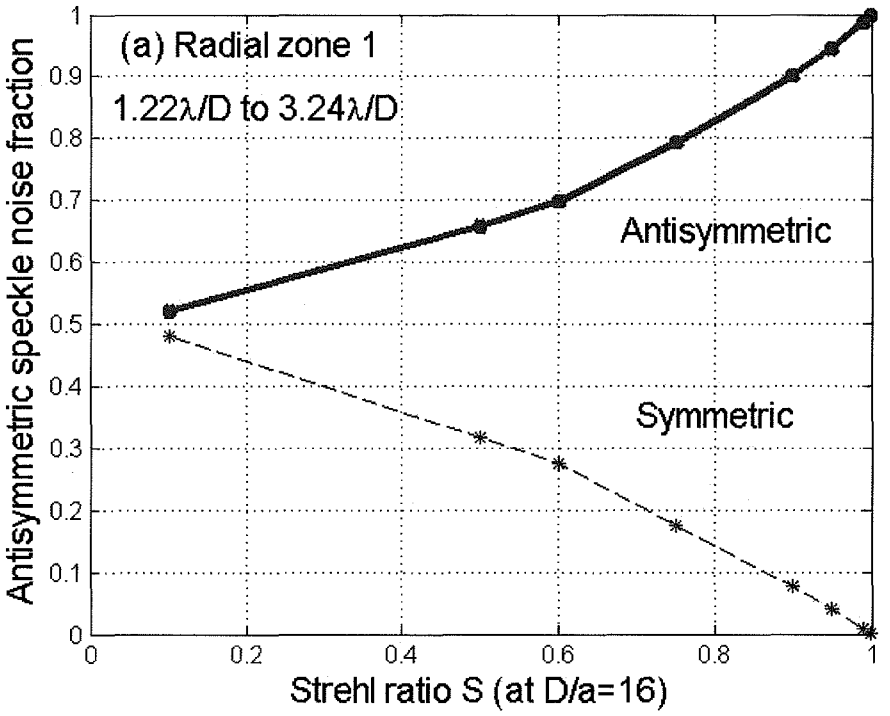

Figure 4 – Dependence of the spatially antisymmetric speckle noise variance fraction (solid curve) on Strehl ratio, S, for D/a=16. Departure from 0.5 signals exotic speckle effects (high symmetry or antisymmetry, the latter also implying speckle pinning). Data points are averages of monochromatic small-pixel values over the inner two Airy rings of the halo, between nulls at 1.22 λ/D and 3.24 λ/D. Plotted points are for S= 0.1, 0.5, 0.6, 0.75, 0.9, 0.95, 0.99, 0.999. At low S, speckle patterns lack distinct spatial symmetry, and the antisymmetric noise variance fraction is approximately 0.5. At highest S, the linear term $2\,\mathrm{Re}\{i\overline{A}^{*}\,\overline{\phi}\}$ always dominates, boosting antisymmetric speckle intensity and noise. Noise variance fractions can be even more dramatic for small, narrowband pixels on Airy nulls, where the linear term vanishes; large, broadband pixels preferentially suppress the antisymmetric component as contributions from the signed linear term partially cancel.

Very high correction (S=0.95, D/a=16) has recently been achieved by projecting the Palomar adaptive optics system onto an unobscured 1.5-meter subaperture of the 5 meter Hale telescope[14]. (This configuration optimizes performance of an FQPM coronagraph.) Under these conditions, the numerical simulations of Fig. 4 indicate that the antisymmetric noise variance fraction averaged over the innermost two Airy rings of the speckle halo is about 0.95. Blocking this dominant symmetry component would reduce speckle noise by a factor of 4.5, resulting in an overall SNR improvement of 2.2 when the reduction of companion signal by image symmetrization is taken into account. If Strehl were further improved to S=0.99, the data of Fig. 4 indicate the antisymmetric noise variance fraction would increase to 0.987, giving a SNR improvement factor of 4.4. The results of Fig. 4 agree with estimates from Equations (1)-(4) and past modelling of symmetric noise reduction[2,3,10], but not, as discussed near the end of §1, with past speckle noise estimates that generally neglected the diffraction cross-term, $2\,\mathrm{Re}\{i\overline{A}^{*}\,\overline{\phi}\}$, representing antisymmetric, linear-term speckles. The estimates of Equations (1)-(4) can be used to calculate the expected antisymmetric noise variance fraction, as a check on the values found numerically. The symmetric and antisymmetric image components are approximated by the dominant terms in each case, the quadratic and linear terms in Equation (2), and the noise variances are proportional to the square of the image components as given in Equation (1). The antisymmetric noise variance fraction is then

$$f = \frac{\sigma^2_{anti}}{\sigma^2_{anti} + \sigma^2_{symm}} = \left[1 + \frac{\sigma^2_{symm}}{\sigma^2_{anti}}\right]^{-1} \approx 1 - \frac{\sigma^2_{symm}}{\sigma^2_{anti}} \approx 1 - \frac{F^2_{symm}}{F^2_{anti}} \approx 1 - \frac{1}{2\langle|\overline{A}|^2\rangle}\frac{1-S}{0.342}\left(\frac{a}{D}\right)^2 \quad . \tag{5}$$

For the correction values considered immediately above, S=0.99 and D/a=16, on the inner two Airy rings (radial zone 1 as defined in Fig. 4, where the average PSF value $<|\overline{A}|^2>$ is 0.0045), these approximations predict an antisymmetric noise variance fraction of ~0.987, in close agreement with the value found from the numerical results just discussed. The dependences displayed analytically in Equation (5) allow extrapolation to even more extreme adaptive parameters, where the antisymmetric noise fraction is larger still. For example, if the actuator density were scaled to D/a=100 at S=0.99, these simple estimates would predict an antisymmetric noise variance fraction of ~0.99967, presenting a potential improvement in speckle-noise-limited companion-detection SNR of almost a factor of 28.

A number of points concerning these results should be kept in mind. First, the speckle noise that is eliminated by the proposed image processing is in excess of traditional speckle noise estimates based on the total speckle power in an image, (1-S). So ultimate speckle-noise-limited sensitivity is being improved to these classical expectations but not beyond. Second, averaging speckles over broad wavelength bands or over large detector pixels can have different effects on the two speckle symmetry classes, and would probably tend to reduce antisymmetric speckle noise preferentially. Third, for relatively faint stars and short integration times, shot noise on the Airy pattern can dominate speckle noise, reducing the practical effectiveness of the sensitivity gains described here. For some experimental situations, however, rather large reductions in speckle noise are possible through image symmetrization.

4. SPECKLE SYMMETRY IN CORONAGRAPHS

The most promising approaches to searching for faint companions use coronagraphs to suppress the light from the bright central star. A speckle algebraic formalism closely analogous to that presented earlier for simple adaptive images applies to this case. If the coronagraph is space-based, speckles will arise in aberrations in beamtrain optics and evolve much more slowly than the speckles caused by atmospheric turbulence seen at ground-based observatories. In any coronagraph, the focal plane image is[15]

$$I(x,y) \approx \left|\overline{\overline{pfA[1+i\phi]}}\right|^2 = \left|\overline{\overline{pfA}}\right|^2 + 2\,\mathrm{Re}\left\{i\left(\overline{\overline{pfA}}\right)^*\left(\overline{\overline{pf\phi}}\right)\right\} + \left|\overline{\overline{pf\phi}}\right|^2 \quad , \tag{6}$$

where pupil-plane (Lyot) and focal-plane spatial masks are represented by multiplicative complex two-dimensional functions p and f, respectively. The focal-plane mask may be an opaque spot, as with the classical Lyot coronagraph, or an arrangement of phase-shifting quadrants, as in the FQPM (four-quadrant phase mask) coronagraph. By design, coronagraphs suppress light from the on-axis star. The first term on the right side of Equation (6), normally an Airy pattern, is suppressed by a large factor that is a function of spatial position in the focal plane. This may conveniently be expressed in a phenomenological way by writing

$$\left|\overline{\overline{pfA}}\right|^2 \sim \frac{\left|\overline{A}\right|^2}{R} \quad , \tag{7}$$

where R is a (possibly large) positive number that varies with position in the focal plane. (This picture is a great simplification, as Airy rings are generally both suppressed and shifted in position by a coronagraph, but it provides a useful framework for gross estimation of speckle magnitudes.) Coronagraph contrast of 10^{-7} at 4.5λ/D has been reported[16], roughly equivalent to R=7800.

Generally, the intensities of quadratic-term speckles (described by the 3rd term on the right side of Equation 6) are little changed by passage through a coronagraph: their peaks are only slightly reduced as their light is distributed over a diffraction-limited diameter that is slightly broadened by the reduced pupil diameter of the Lyot stop. On the other hand, linear-term speckles (recognizable as the 2nd term on the right side of Equation 6) are substantially reduced in intensity by the coronagraphic suppression of light from the on-axis star. Crudely speaking, from Equations (6) and (7), linear-term speckle intensity is reduced[15,17] by a factor $\sqrt{R}$, which describes the reduction of Airy amplitude. Speckle noise is still proportional to typical speckle intensity, as described by Equation (1).

Linear-term speckles are entirely neglected if suppression R is assumed infinite[18,19]; but in real coronagraphs they would still dominate at correction sufficiently high that $|\bar{\phi}|^2 < |\bar{A}|^2/R$. This is a much more stringent condition requiring much higher correction than the analogous condition for adaptively corrected simple imaging, $|\bar{\phi}|^2 < |\bar{A}|^2$. So at any but the highest correction, or in the limit of high coronagraph suppression, speckle patterns in the coronagraph case are predominantly symmetric because linear-term speckles are suppressed. Simple image processing based on speckle symmetry is again effective in reducing speckle noise, but it will involve image antisymmetrization rather than symmetrization. When quadratic-term speckles are rejected by this processing, the speckle intensity floor or contrast will be defined by the intensity of the linear term. As before, half the signal in any companion image is lost, but speckle noise is reduced much more.

The calculations represented by Fig. 4 are easily converted to find the fraction of speckle noise variance in a coronagraph, for various S, D/a, that is spatially symmetric. The antisymmetric portion must be divided by R to represent coronagraphic suppression of linear-term speckles:

$$f' = \frac{\sigma^2_{symm}}{\sigma^2_{anti}/R + \sigma^2_{symm}} = \frac{R(1-f)}{f + R(1-f)} \quad . \tag{8}$$

This expression reduces to (1-f) as it should when R=1 (the simple imaging case); it reaches f'=0.987 when f=0.99 and R=7800. That is, the coronagraph has converted a large antisymmetric speckle variance fraction f into a large symmetric speckle variance fraction f' by suppressing linear-term speckles.

An additional benefit of image processing to antisymmetrize coronagraph images is the rejection of speckle noise from amplitude speckles $2\mathrm{Re}\{\bar{A}^*\overline{\delta A}\}$ and $|\overline{\delta A}|^2$, both of which are spatially symmetric. Amplitude speckles are generated by intensity variations across the pupil; unlike phase speckles, they cannot easily be corrected over a broad spectral band[20] by the "speckle nulling" technique that uses targeted commands on the deformable mirror to achieve spectacular suppression of phase speckles[21]. The very simple image processing described here is equally effective on amplitude speckles because they have the same spatial symmetry as the dominant quadratic-term phase speckles.

5. CONCLUSIONS

The symmetry properties of speckles at high adaptive correction have been reviewed, and the degree of symmetry as a function of image correction has been presented. Symmetry content of the speckle halo is found to be considerable at degrees of adaptive correction that will be accessible in "extreme" adaptive optics of the near future. Under these conditions, a substantial reduction of speckle noise can be achieved by simple post-processing of images to reject the spatially antisymmetric component. Though generally reducing the image signature from a companion by a factor of 2, this simple technique also reduces speckle noise by a much larger factor, as indicated by numerical simulations and simple speckle intensity estimates. For example, as shown in §3, correction conditions of S=0.99 and D/a=100 will allow improvement of the net companion-detection SNR by a factor of 28. Analogous techniques are effective with coronagraphs, where symmetric rather than antisymmetric speckles dominate. Though this approach is still subject to shot noise on Airy rings and the pre-suppression speckles, the sensitivity gain it offers is extremely simple to implement.

ACKNOWLEDGMENTS

The research described in this publication was carried out at the Jet Propulsion Laboratory, California Institute of Technology, under a contract with the National Aeronautics and Space Administration.

REFERENCES

1. J. R. P. Angel, "Ground-based imaging of extrasolar planets using adaptive optics", *Nature* **368**, pp. 203-207, 1994.
2. D. Rouan, P. Riaud, A. Boccaletti, Y. Clénet, and A. Labeyrie, "The four-quadrant phase-mask coronagraph. I. principle", *Pub. Astron. Soc. Pac.* **112**, pp. 1479-1486, 2000.
3. A. Boccaletti, P. Riaud, and D. Rouan, "Speckle symmetry with high-contrast coronagraphs", *Pub. Astron. Soc. Pac.* **114**, pp. 132-136, 2002.
4. E. E. Bloemhof, "Suppression of speckle noise by speckle pinning in adaptive optics", *Ap. J.* **582**, pp. L59-L62, 2003.
5. J. J. Lissauer, "Extrasolar planets", *Nature* **419**, pp. 355-358, 2002.
6. R. Racine, G. A. H. Walker, D. Nadeau, R. Doyon, and C. Marois, "Speckle noise and the detection of faint companions", *Pub. Astron. Soc. Pac.* **111**, pp. 587-594, 1999.
7. R. N. Bracewell, "The Fourier Transform and Its Applications", 2nd ed. (McGraw-Hill, New York, 1986).
8. F. Roddier, "The effects of atmospheric turbulence in optical astronomy", *Prog. in Optics* **19**, pp. 281-376, 1981.
9. E. E. Bloemhof, R. G. Dekany, M. Troy, and B. R. Oppenheimer, "Behavior of remnant speckles in an adaptively corrected imaging system", *Astrophys. J.* **558**, pp. L71-L74, 2001.
10. A. Sivaramakrishnan, P. E. Hodge, R. B. Makidon, M. D. Perrin, J. P. Lloyd, E. E. Bloemhof, and B. R. Oppenheimer, "The Adaptive Optics Point-Spread Function at Moderate and High Strehl Ratios", *Proc. SPIE* **4860**, pp. 161-171, 2003.
11. E. E. Bloemhof, "Anomalous intensity of pinned speckles at high adaptive correction", *Opt. Lett.* **29**, pp. 159-161, 2004.
12. J. W. Goodman, "Introduction to Fourier Optics" (McGraw-Hill, New York, 1968).
13. M. Troy, R. G. Dekany, B. R. Oppenheimer, E. E. Bloemhof, T. Trinh, F. Dekens, F. Shi, T. L. Hayward, and B. Brandl, "Palomar Adaptive Optics Project: Status and Performance", *Proc. SPIE* **4007**, pp. 31-40, 2000.
14. P. Haguenauer, E. Serabyn, E. E. Bloemhof, J. K. Wallace, R. O. Gappinger, B. P. Mennesson, M. Troy, C. D. Koresko, and J. D. Moore, "An off-axis four-quadrant phase-mask coronagraph for Palomar: high contrast near bright stars imager", *Proc. SPIE* **5905**, pp. 59050S-1--59050S-11, 2005.
15. E. E. Bloemhof, "Remnant Speckles in a Highly Corrected Coronagraph", *Ap.J.* **610**, pp. L69-L72, 2004.
16. A. Chakraborty, L. A. Thompson, and M. Rogosky, "10^{-7} contrast ratio at 4.5λ/D: New results obtained in laboratory experiments using nanofabricated coronagraph and multi-Gaussian shaped pupil masks", *Opt. Express* Vol. **13**, No. 7, 2394-2402, 2005.
17. C. Aime and R. Soummer, "The usefulness and limits of coronagraphy in the presence of pinned speckles", *Astrophys. J.* **612**, L85-L88, 2004.
18. F. Malbet, J. W. Yu, and M. Shao, "High-dynamic-range imaging using a deformable mirror for space coronagraphy", *Publ. Astron. Soc. Pacif.* **107**, 386-398, 1995.
19. S. Shaklan, D. Moody, and J. Green, "Residual wave front phase estimation in the reimaged Lyot plan for the Eclipse coronagraphic telescope", *Proc. SPIE* **4860**, 361-370, 2003.
20. A. Quirrenbach, "Coronagraphic methods for the detection of terrestrial planets", preprint at (http://arXiv.org/astro-ph/0502254), 2005.
21. J. Trauger, C. Burrows, B. Gordon, J. Green, A. Lowman, D. Moody, A. Niessner, F. Shi, and D. Wilson, "Coronagraph contrast demonstrations with the high-contrast imaging testbed", *Proc SPIE* **5487**, 1330-1336, 2004.